INVESTIGATION OF MAGNETOHYDRODYNAMICS FLOW AND HEAT TRANSFER IN THE PRESENCE OF A CONFINED SQUARE CYLINDER USING SM82 EQUATIONS

by

Mohammad FARAHI SHAHRI and Alireza HOSSEIN NEZHAD*

Department of Mechanical Engineering, University of Sistan and Baluchestan, Zahedan, Iran

Original scientific paper
https://doi.org/10.2298/TSCI140313048F

In this paper, magnetohydrodynamics flow and heat transfer of a liquid metal (GaInSn) in the presence of a confined square obstacle is studied numerically, using a quasi-2-D model known as SM82. The results of the present investigation are compared with the results of the other experimental investigations and a good agreement with the average deviation of about 2.8% is achieved. The effects of Reynolds number, Hartmann number, and blockage ratio on the re-circulation length, Strouhal number, averaged Nusselt number, and isotherms are examined. The numerical results indicate that based on the Reynolds and Hartmann numbers in a fixed blockage ratio, due to the direct interactions of the secondary vortices and the Karman ones, the Strouhal number may increase or decrease. Some correlations are also provided to determine the re-circulation length in terms of the Reynolds and Hartmann numbers for various blockage ratios.

Key words: *magnetohydrodynamics, square obstacle, Hartmann number, blockage ratio*

Introduction

The study of the MHD flow in the presence of a confined obstacle placed in a rectangular channel, under the influence of an external magnetic field, is of significant practical interest. MHD flows in confined arrangements of obstacles play a major role in a wide range of engineering applications, such as cooling of liquid metal blankets in fusion reactors. Inserting an obstacle in the flow can induce vortices and promote heat transfer rates for these applications. Therefore, recognizing the promotion or suppression of flow instabilities, and the generation of secondary flows can provide helpful knowledge of practical importance.

Under a sufficiently strong magnetic field, the liquid metal interacts with the external magnetic field in such a way that parallel disturbances to the magnetic field are strongly suppressed, giving vortices a tendency to elongate parallel with the magnetic field [1, 2]. Therefore these MHD duct flows consist of a 2-D core flow confined by boundary layers on the duct walls. At the walls perpendicular to the magnetic field, thinner boundary layers (Hartmann layers) grow, which exert a friction on the core 2-D flow, leading to the development of quasi-two-dimensional (Q2-D) model, called SM82 for these flows [1]. The observa-

* Corresponding autor, email: nezhadd@hamoon.usb.ac.ir

tions of [3] showed that even at high Reynolds numbers, the MHD damping effects can laminarize the flow to a state that is well-described by a Q2-D model, provided that the Hartmann numbers are satisfactorily high. A noticeable benefit of this model is that it can lessen the computational costs of a 3-D problem by changing it to a 2-D one. Most of the performed simulations of MHD flows in such complex environments rely on this model due to the high computational costs of 3-D simulations.

Several studies in the literature deal with MHD flows, where the magnetic field is aligned with the confined cylinder axis. It is shown that for moderate and high Hartmann numbers (Ha $\geq$ 320), the onset of vortex shedding is postponed till higher Reynolds numbers [4-7]. For a certain blockage ratio β (the ratio of the blockage length to the channel width), a linear dependence of the corresponding critical Reynolds number on Hartmann number has been observed [4-6]. This has encouraged some investigations into the instability and turbulent transition in MHD duct flows such as [7, 8]. Hussam *et al.* [5] carried out a parametric study and observed furthermore that with increasing β, the slope of the critical Reynolds number curve is increased. They also studied a subsequent numerical investigation whereby a torsional oscillation was imparted on a cylinder located within a Q2-D duct flow to encourage vortex shedding and enhance heat transfer from the heated wall of the duct [9]. By increasing further the Reynolds number, experiments from [6] and numerical simulations of [4] have discovered the presence of a novel flow regime that follows the laminar periodic vortex shedding and does not have an equivalent in the purely hydrodynamic case. In this regime, the flow is distinguished by irregular vortex shedding patterns, with secondary vortices being separated from the channel walls [4]. Again, as the imposed magnetic field is increased; transition to this regime is postponed. Muck *et al.* [9] showed that for Stuart numbers in the range $2 \leq N \leq 10$, transition from a time-dependent 3-D flow to a 2-D state occurred.

Most of the studies in the literature have been based on the Q2-D model, whose validity is limited to high Hartmann and Stuart numbers. The main objective of [10] was to fill in the gap in the area of low Hartmann number for this type of flows. To recognize that, a fully 3-D direct numerical simulation was used to assess independently the performance and range of validity of simplified models, such as the Q2-D model. Recently [11] performed quasi-2-D simulations of MHD flow around a circular cylinder aligned with the magnetic field which was offset from the duct centerline. They showed that by offsetting the cylinder from the wake centerline, heat transfer enhancement of up to 48% is achieved.

However, Muck *et al.* [9] performed 3-D simulations of MHD flow around a square cylinder, but in that case an analytical wall boundary model was used, a fact that not allowed the resolution of the thin Hartmann layers, therefore making impossible the detailed analysis of the interaction between the vortices and the channel walls. Moreover, because of available computer resources restrictions at that time, only two Reynolds numbers could be studied (Re = 200 and 250), and the Hartmann number was varied in the range of $63 < \text{Ha} < 850$. So the present work is motivated by the lack of detailed simulations addressing the case of confined MHD flows around a square obstacle using SM82 model. Due to the importance of the heat transfer in such problems, in this paper combined MHD flow and heat transfer of a liquid metal around an obstacle with square cross-section which is confined in a channel and under a strong magnetic field are investigated in $1 \leq \text{Re} \leq 3000$, $300 \leq \text{Ha} \leq 1200$, $\gamma = a/h = 0.5$, and Pr = 0.022. Moreover the effects of blockage ratio ($0.1 \leq \beta \leq 0.4$) is considered here, which is not contributed in [9].

Problem statement

Liquid metal (GaInSn) in a rectangular channel in the presence of a confined square cylinder is considered. As shown in fig. 1, h is the channel width and $a = h/2$ is the channel height. The uniform magnetic field B acts along the cylinder axis (z-axis). The temperature of the front wall is constant and equal to $T_{w1} = T_w$ and the temperature of the rear wall is $T_{w2} = T_0$. In this condition, thermal convection can and will develop in the presence of temperature difference between sidewalls. The upper and lower walls of the channel are thermally insulated and all of channel walls and obstacle surfaces are electrically insulated. At the entrance, the velocity profile is assumed to be fully developed and the fluid temperature is $T_{in} = T_0$. The cylindrical obstacle with square cross-section with the chord length of d is placed at an equal distance to the front and rear walls of the channel. The blockage ratio is defined as $\beta = d/h$.

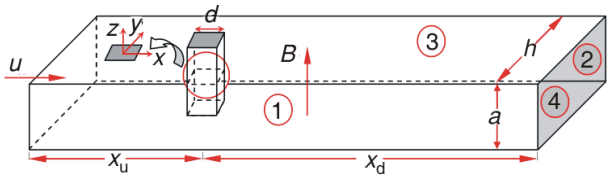

Figure 1. Physical model and the co-ordinate system
(1) front wall (constant temperature, T_{w1}), (2) rear wall (constant temperature, T_{w2}), (3) upper wall (adiabatic), (4) lower wall (adiabatic)

Due to the physical properties of GaInSn [12], the magnetic Reynolds number (the ratio of the induced magnetic field to the external magnetic field) is so small ($Re_m \ll 1$). In this condition, the induced magnetic field effects can be neglected compared to the external magnetic field. Assuming large Hartmann and Stuart numbers (Ha $\gg$ 1 and N $\gg$1), by averaging the Navier-Stokes equations in the direction of the magnetic field (z-axis), a Q2-D model for the MHD flow and heat transfer through the channel, in the *x-y* plane (perpendicular plane to the magnetic field) is obtained [1]. In this model, the effects of Hartmann layers are included in the momentum equations as a source term and known as Hartmann braking term. Also by averaging the 3-D energy equation in the z-direction and by considering the Joule heating source term in it, energy equation is obtained in the x-y plane.

Governing equations and boundary conditions

According to the mentioned assumptions and discussions, the governing equations (including continuity, momentum and energy equations) in the x–y plane are:

$$\nabla \bar{\vec{u}} = 0 \tag{1}$$

$$\frac{\partial \bar{\vec{u}}}{\partial t} + (\bar{\vec{u}} \cdot \nabla)\bar{\vec{u}} + \frac{1}{\rho}\nabla \bar{p} = \nu \nabla^2 \bar{\vec{u}} - \frac{2B}{a}\frac{\sigma \nu}{\rho}\bar{\vec{u}} \tag{2}$$

$$\rho c_P \frac{\partial \bar{T}}{\partial t} + \rho c_P (\bar{\vec{u}} \cdot \nabla)\bar{T} = k\nabla^2 \bar{T} + \sigma B^2 \bar{u}^2 \tag{3}$$

where ν is the kinematic viscosity, ρ – the density, c_p – the specific heat capacity, k – the thermal conductivity, and σ – the electrical conductivity of the fluid. Also the average pressure, temperature and velocity fields in z-direction are obtained using the relations:

$$\bar{\mathrm{u}} = \frac{1}{a}\int_{z=0}^{z=a} \mathrm{u}\,\mathrm{d}z, \quad \bar{p} = \frac{1}{a}\int_{z=0}^{z=a} p\,\mathrm{d}z, \quad \bar{T} = \frac{1}{a}\int_{z=0}^{z=a} T\,\mathrm{d}z \tag{4}$$

To make the mentioned equations dimensionless, the following dimensionless variables are used:

$$\nabla_{\mathrm{nd}} = d\nabla, \quad t_{\mathrm{nd}} = \frac{u_0}{d}t, \quad \vec{\mathrm{U}} = \frac{\vec{\bar{\mathrm{u}}}}{u_0}, \quad P = \frac{\bar{p}}{\rho u_0^2}, \quad \theta = \frac{\bar{T} - T_0}{T_{\mathrm{w}} - T_0} \tag{5}$$

It is necessary to note that hereafter; the lengths have been reported to d. By substituting the dimensionless quantities into (1-3), the dimensionless governing equations are obtained:

$$\nabla_{\mathrm{nd}} \cdot \vec{\mathrm{U}} = 0 \tag{6}$$

$$\frac{\partial \vec{\mathrm{U}}}{\partial t_{\mathrm{nd}}} + (\vec{\mathrm{U}} \cdot \nabla_{\mathrm{nd}})\vec{\mathrm{U}} + \nabla_{\mathrm{nd}} P = \frac{1}{\mathrm{Re}}\nabla_{\mathrm{nd}}^2 \vec{\mathrm{U}} - 2\frac{d^2}{a^2}\frac{\mathrm{Ha}}{\mathrm{Re}}\vec{\mathrm{U}} \tag{7}$$

$$\frac{\partial \theta}{\partial t_{\mathrm{nd}}} + (\vec{\mathrm{U}} \cdot \nabla_{\mathrm{nd}})\theta = \frac{1}{\mathrm{RePr}}\nabla_{\mathrm{nd}}^2 \theta + J\,\vec{\mathrm{U}}^2 \tag{8}$$

In the previous equations, Reynolds number, Prandtl number, Hartmann number, and Joule heating parameter are defined as:

$$\mathrm{Re} = \frac{u_0 d}{\nu}, \quad \mathrm{Pr} = \frac{\mu c_{\mathrm{p}}}{k}, \quad \mathrm{Ha} = aB\sqrt{\frac{\sigma}{\mu}}, \quad J = \frac{\sigma B^2 u_0 d}{\rho c_{\mathrm{p}} \Delta T} \tag{9}$$

It should be noted that based on the physical properties of GaInSn [12], the value of Joule heating parameter (J) is very small (approximately $5 \cdot 10^{-5}$) in this study, so Joule heating term is neglected in the energy equation compared to the other terms. Considering both upper and lower walls of the channel are electrically and thermally insulated, the hydrodynamic and thermal boundary conditions are:

Boundary conditions at entrance: Assuming MHD fully developed flow [4] and a known temperature at the inlet, the dimensionless velocity profile and the dimensionless temperature are:

$$U\left(-\frac{x_{\mathrm{u}}}{d}, Y\right) = \frac{\cosh\left(Y\frac{d}{a}\sqrt{2\mathrm{Ha}}\right) - \cosh\left(\frac{h}{2a}\sqrt{2\mathrm{Ha}}\right)}{1 - \cosh\left(\frac{h}{2a}\sqrt{2\mathrm{Ha}}\right)}, \quad V = 0, \quad \theta = 0 \tag{10}$$

Boundary conditions at the front wall of the channel:

$$\vec{\mathrm{U}}\left(X, -\frac{h}{2d}\right) = 0, \quad \theta\left(X, -\frac{h}{2d}\right) = 1 \tag{11}$$

Boundary conditions at the rear wall of the channel:

$$\vec{\mathrm{U}}\left(X, +\frac{h}{2d}\right) = 0, \quad \theta\left(X, +\frac{h}{2d}\right) = 0 \tag{12}$$

Boundary conditions at the exit: by choosing appropriate upstream and downstream distances, the fully developed boundary condition is used:

$$\frac{\partial U}{\partial X}=0,\quad \frac{\partial V}{\partial X}=0,\quad \frac{\partial \theta}{\partial X}=0 \tag{13}$$

The obstacle boundary conditions:

$$\vec{\mathrm{U}}(X,Y)\Big|_{C^*}=0,\qquad \vec{\mathrm{n}}\cdot\nabla_{\mathrm{nd}}\ \theta\Big|_{C^*}=0 \tag{14}$$

where C^* represents a boundary which is encompassed the obstacle surface.

Numerical procedure

Equations (6)-(8) with eqs. (10)-(14) are solved using the finite volume method. For the coupling of velocity and pressure fields, the SIMPLE algorithm and for the temporal discretization, the second order implicit time scheme with time intervals of Δt = 0.05 are employed. Finally a computer program is developed for solving the discrete equations in a computational domain as shown in fig. 2. As seen in this figure 0.25 units away from the obstacle surface and channel walls, a uniform mesh distribution with the smallest distance between grid lines (δ), is used.

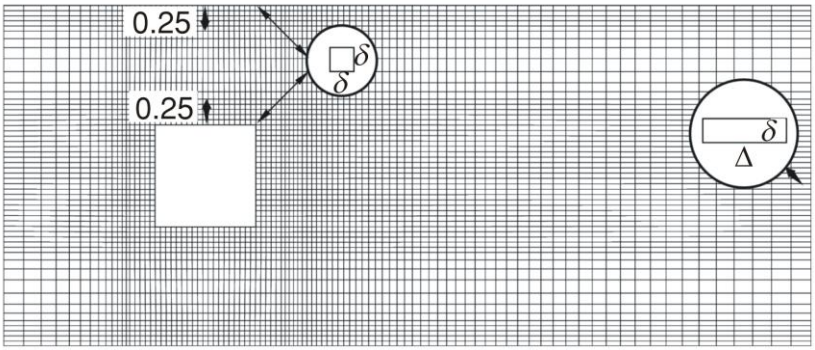

Figure 2. Schematic of the computational domain

Away from the obstacle surface and toward the inlet and outlet of the channel in the x-direction, the spacing between grid lines extends so that at areas near inlet and outlet, the non-uniform mesh distribution with the largest distance between the grid lines (Δ = 0.06) can be used. For stretching the cell sizes between the limits of δ and Δ in the x-direction, the hyperbolic tangent function has been used [13]. Also using an algebraic expression [14], the vertical grid lines extend from the 0.25 units away from the obstacle surface and the channel walls in the y-direction.

The upstream and downstream distances are selected based on extensive studies conducted on their effects on the drag coefficient, C_{D}, Strouhal number, St, and average Nusselt number, $\mathrm{Nu}_{\mathrm{avg}}$. These studies are conducted for six Reynolds numbers (Re = 500, Re = 1000, Re = 1500, Re = 2000, Re = 2500, and Re = 3000), four Hartmann numbers (Ha = 300, Ha = 600, Ha = 900, and Ha = 1200), four blockage ratio (β = 0.1, β = 0.2, β = 0.3, and β = 0.4), and a fixed Prandtl number (Pr = 0.022).

The largest changes in the C_D, St, and Nu_{avg} due to variations of the upstream and downstream distances (X_u and X_d) occur at Re = 3000, Ha = 300, $\beta = 0.1$, and Pr = 0.022. Considering these values and by choosing $X_d = 36$, variations of C_D, St, and Nu_{avg} in terms of X_u, are presented in tab. 1. As shown in this table, by passing from $X_u = 8$ to $X_u = 12$, changes in C_D, St, and Nu_{avg} are negligible; So $X_u = 8$ is selected as the upstream distance. Similarly in $X_u = 8$ passing the downstream distance from $X_d = 26$ to $X_d = 36$ results in minimal change in the C_D, St, and Nu_{avg}. So $X_d = 26$ is selected as the downstream distance.

Table 1. Effects of upstream distance on C_D, St, and Nu_{ave} at Re = 3000, Ha = 300, β=0.1, γ= 0.5, and Pr = 0.022 for X_d = 36

X_u	C_D	St	Nu_{ave}
4	1.7186	0.8357	3.7648
8	1.7165	0.8344	3.7632
12	1.7158	0.8339	3.7628
16	1.7153	0.8336	3.7626

Table 2. Effects of different grid structures on C_D, St, and Nu_{avg} for Re = 3000, γ= 0.5, Ha = 300, and Pr = 0.022

Grids	δ	β = 0.1				β = 0.4			
		No. of cells	C_D	St	Nu_{avg}	No. of cells	C_D	St	Nu_{avg}
G_1	0.08	21029	1.717	0.834	3.763	15670	2.857	1.248	5.659
G_2	0.04	43564	1.592	0.351	2.458	36454	2.367	1.049	3.988
G_3	0.02	75986	1.554	0.311	2.345	61100	2.327	1.033	3.963
G_4	0.01	90240	1.553	0.310	2.345	89425	2.327	1.032	3.963

To check the effects of grid structure, studies similar to the domain independence ones are performed for four types of grids G_1, G_2, G_3, and G_4. The maximum variations of C_D, St and Nu_{avg} are observed at Re = 3000, Ha = 300, and Pr = 0.022. As shown in tab. 2, by passing from G_3 to G_4, the values of C_D, St, and Nu_{avg} change 0.23, 0.66, and 0.34% for $\beta = 0.1$, and 0.14, 0.35, and 0.25% for $\beta = 0.4$, respectively. So considering the tradeoff between the accuracy and the computational costs, the G_3 ($\delta = 0.02$) grid type is adopted for this work.

In order to verify the numerical procedure, the present results for the critical Reynolds number in $\beta = 0.1$ and $\gamma = 0.5$ for different Hartmann numbers are compared with the experimental results of [6]. As shown in fig. 3, the present results are in good agreement with those of [6] and the average deviation between them is about 2.8%. This deviation is the result of using a non-intrusive measurement device to calculate the core flow quantities by measuring the electric potential only at one Hartmann wall in [6].

Results and discussion

For better understanding of the flow structure, streamlines for Re = 600, $\gamma = a/d$ = = 0.5, and $\beta = 0.2$ at different Hartmann numbers are presented in fig. 4.

As seen in this figure, at Ha = 300 an additional flow regime that does not have a counterpart in the purely hydrodynamic case is appeared.

This regime is specific to confined cylinder wakes, in which the boundary layers at the side walls are likely to separate and generate vortex shedding. In this case, the Karman vortices are still initiated as in the purely hydrodynamic case, but at the side walls secondary vortices are generated, shed and eventually flowed downstream. With further increase of the Hartmann number (Ha = 1200), the vortex shedding process is completely suppressed and the unsteady flow is moved toward a steady one. In this situation a closed steady re-circulation region characterized by the formation of two symmetric vortices behind the cylinder is observed. Accordingly, the re-circulation length (L_b) can be defined as the distance between the rear stagnation point of the cylinder and the end of the recirculation region.

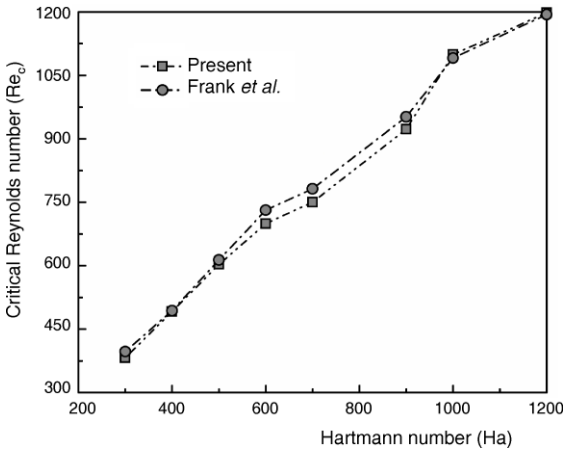

Figure 3. Critical Reynolds number (Re_c) for the onset of unsteady flow regime in β = 0.1 and γ = 0.5, at different Hartmann numbers

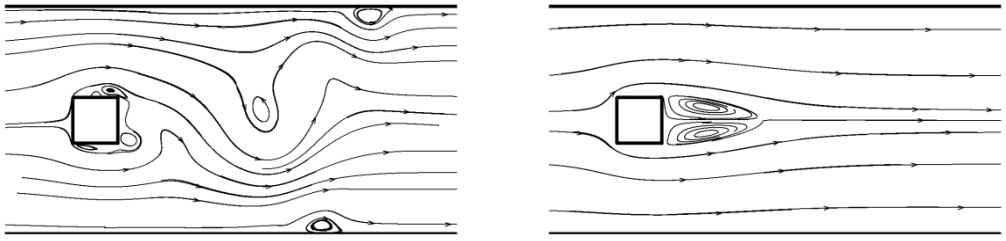

(a) Ha = 300 (b) Ha = 1200

Figure 4. Streamlines for Re = 600, γ = 0.5, and β = 0.2 at different Hartmann numbers

Strouhal number is defined as St = fd/u_0, where f represents the frequency of vortex shedding. Figure 5 shows the variations of Strouhal number *vs.* Reynolds number in different Hartmann numbers and blockage ratios, at γ = 0.5. In general, with increasing of blockage ratio, the Strouhal number is increased, but by varying the Reynolds and Hartmann numbers, the Strouhal number may either increase or decrease. Depending on the values of blockage ratio, Reynolds number and the Hartmann number, it is probable to happen a flow regime in which secondary vortices (as shown in fig. 4) are separated from the bounding walls and enter the Karman vortex street. These vortices act as a barrier against the shedding of Karman vortices and cause a sudden decrease in the frequency of vortex shedding and Strouhal number.

Figure 6 shows the variations of the re-circulation length in terms of $Re/Ha^{0.8}$ at various blockage ratios and γ = 0.5. According to this figure, some correlations, eq. (15), are proposed for the variations of the re-circulation length in terms of $Re/Ha^{0.8}$ at β =0.1, β = 0.2, β = 0.3, and β = 0.4. The maximum and average deviations between the numerical data and the results of correlation are 3.6% and 2.5% for β = 0.1, 3.8%, and 2.53% for β = = 0.2, 3.84% and 2.61% for β = 0.3, and 3.92% and 2.31% for β = 0.4, respectively.

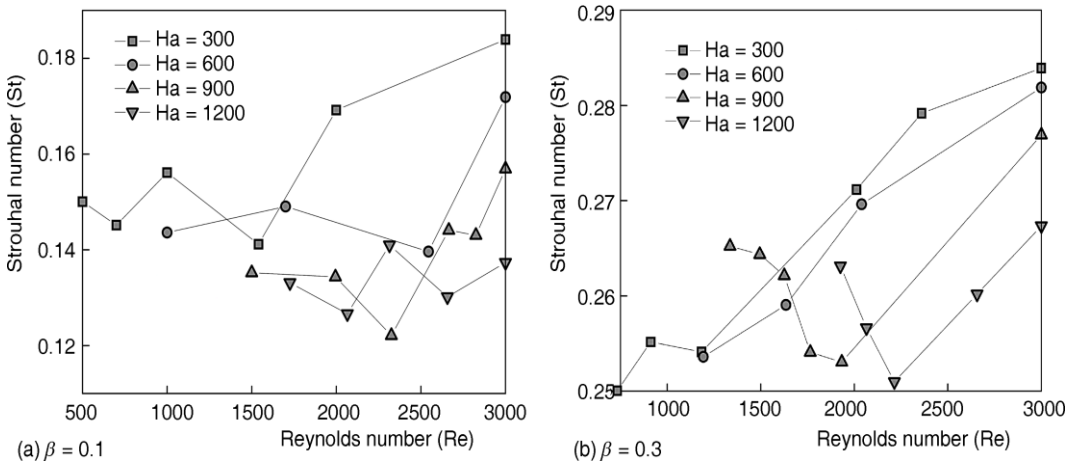

Figure 5. Strouhal number *vs.* Reynolds number at γ = 0.5, for different Hartmann numbers and blockage ratios

$$
\begin{aligned}
L_b &= 0.499\left(\frac{\mathrm{Re}}{\mathrm{Ha}^{0.8}}\right)+0.298 \quad \beta=0.1 \quad 1.129 \le \frac{\mathrm{Re}}{\mathrm{Ha}^{0.8}} \le 1.667 \\
L_b &= 0.478\left(\frac{\mathrm{Re}}{\mathrm{Ha}^{0.8}}\right)+0.321 \quad \beta=0.2 \quad 1.151 \le \frac{\mathrm{Re}}{\mathrm{Ha}^{0.8}} \le 2.246 \\
L_b &= 0.457\left(\frac{\mathrm{Re}}{\mathrm{Ha}^{0.8}}\right)+0.349 \quad \beta=0.3 \quad 1.176 \le \frac{\mathrm{Re}}{\mathrm{Ha}^{0.8}} \le 3.058 \\
L_b &= 0.435\left(\frac{\mathrm{Re}}{\mathrm{Ha}^{0.8}}\right)+0.374 \quad \beta=0.4 \quad 1.198 \le \frac{\mathrm{Re}}{\mathrm{Ha}^{0.8}} \le 4.133
\end{aligned}
\tag{15}
$$

The variation of the average Nusselt number with Hartmann number and blockage ratio, at γ = 0.5, β = 0.2, Re = 1500, and Pr = 0.022 is shown in fig. 7. The heat transfer is shown to be higher at higher blockage ratios. However, Nu_{avg} reduces as Hartmann number is increased from Ha = 300 to Ha = 1200. As the blockage ratio is increased from 0.1 to 0.4, there is a remarkable increase in Nu_{avg} for a constant Hartmann number. This shows that the cylinder can play an important role to enhance the heat transfer rate from the heated wall of the channel.

Figure 8 shows isotherms for Ha = 300 and Ha = 1200 in Re = 1500, β = 0.2, γ = 0.5, and Pr = 0.022. At Ha = 300 the concentration of isotherms is located near the lower heated wall which indicates a noticeable amount of heat transfer from this wall.

Also in this situation, the temperature distribution within the channel is better, in other words the mixing of the cold and hot fluids is occurred effectively in this case. On the contrary in the case of Ha = 1200, the cold and hot fluids mixing is occurred poorly. This in turn results in a heat augmentation on the heated wall. These discussions confirm the results of fig.7 and show that as the Hartmann number increases, the rate of heat transfer from the heated wall is decreased.

The effects of blockage ratio on isotherms in Re = 500, γ = 0.5, Ha = 600, Pr = 0.022 and blockage ratios of 0.1 and 0.4 are shown in fig. 9. According to this figure, at β = 0.1 the cold and hot fluids mixing is very weak and therefore the heat transfer from the heated wall is low.

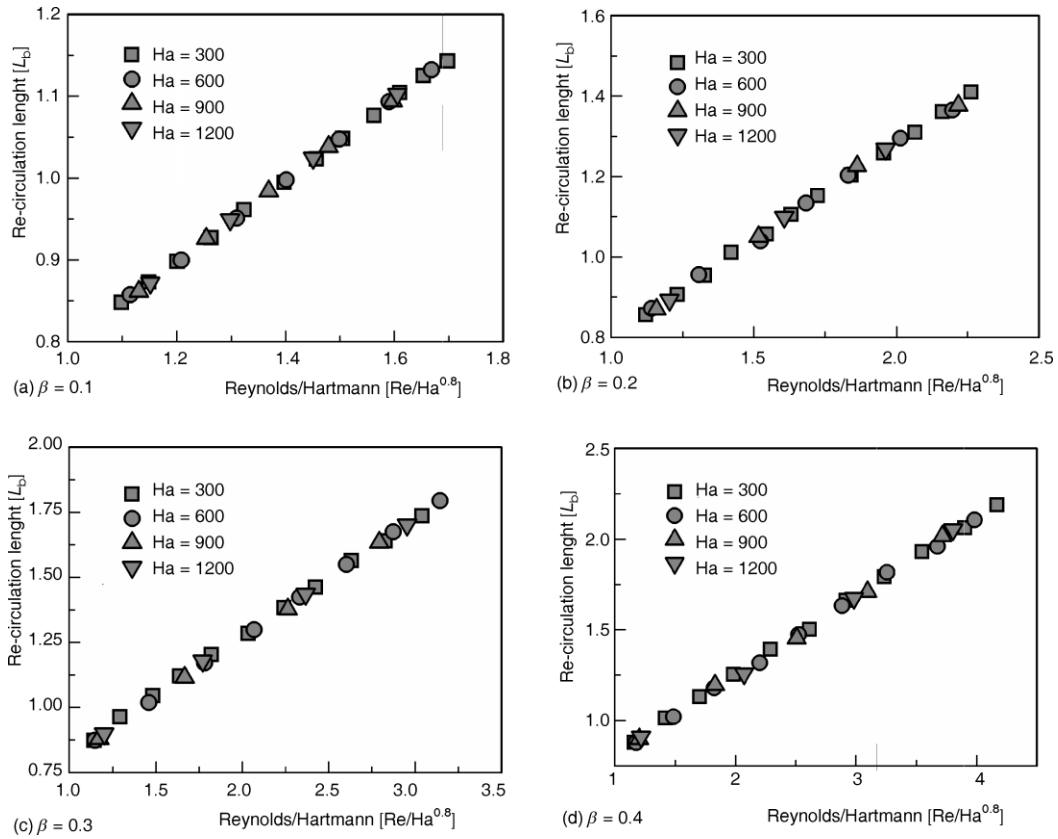

Figure 6. Recirculation length *vs.* Re/Ha$^{0.8}$ in different blockage ratios and γ = 0.5

Actually in this situation, the resulting heat loads imposes thermal stresses to the heated wall. Unfortunately this results in serious damages to the heated wall of the channel. As shown in the fig. 9, at β = 0.4 the cold and hot fluids mixing is occurred more effectively which represents the enhancement of the heat transfer from the heated wall. This allows the temperature of front wall to be controlled by a permitted limit. Interestingly the results of fig. 9 confirm the results of fig. 7 and show that, the increase of blockage ratio enhances the heat transfer from the heated wall of the channel.

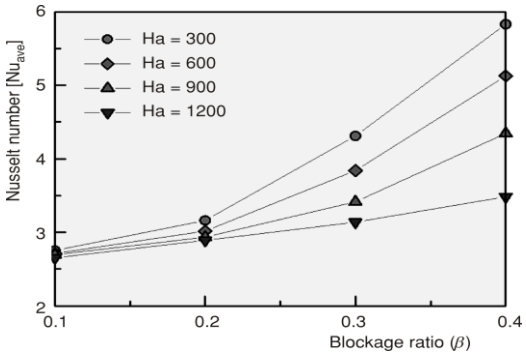

Figure 7. Variation of average Nusslet number as a function of blockage rato at different Hartmann numbers, for γ = 0.5, β = 0.2, Re = 1500, and Pr = 0.022

Conclusions

In this perusal, a numerical investigation has been done for the confined MHD flow and heat transfer in the presence of a square cylinder, using a quasi-2-D model known as SM82. The main achievements of this study are as follows.

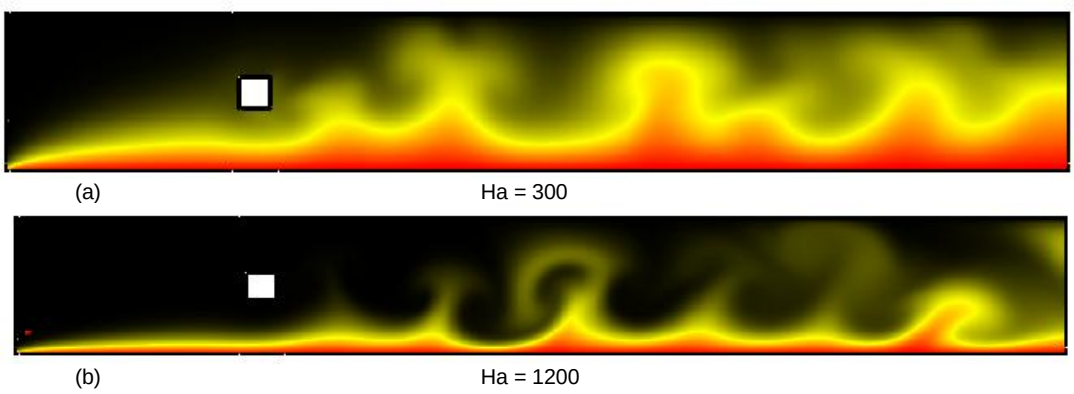

Figure 8. Isotherms for two different Hartmann numbers at γ = 0.5, β = 0.2, Re = 500, and Pr = = 0.022 (dark and light contours correspond, respectively, to colder and hotter regions) (*for color image see journal web site*)

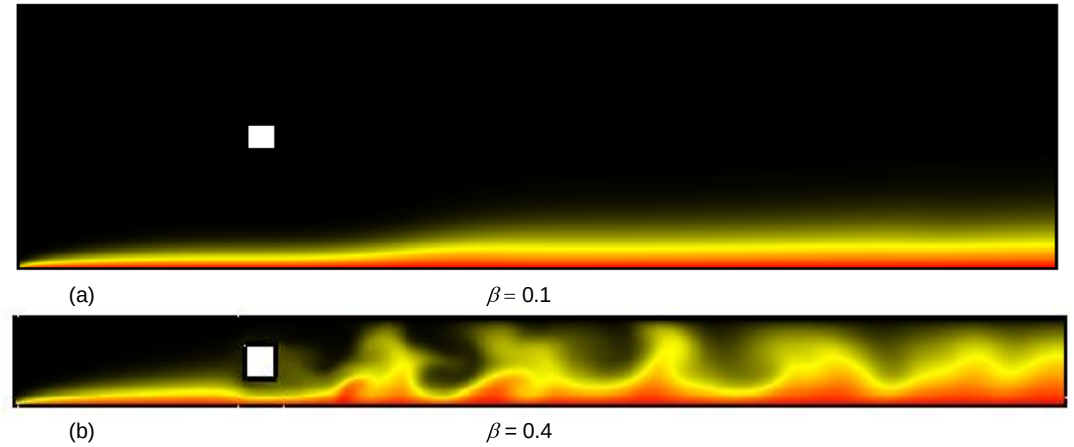

Figure 9. Isotherms for two different blockage ratios at γ = 0.5, Ha = 600, Re = 1500, and Pr =0.022 (contour shading is as per fig. 8) (*for color image see journal web site*)

- At a given blockage ratio, changing each of Reynolds and Hartmann numbers may cause the Strouhal number to decrease or increase. This is due to the separation of the secondary vortices from the channel walls and their interactions with the Karman vortices.
- The average Nusselt number (Nu_{avg}) reduces unavoidably, as the Hartmann number is increased from Ha = 300 to Ha = 1200. In order to enhance heat transfer under these conditions, a confined cylinder can play a significant role to promote the heat transfer rate from the heated wall of the channel. As blockage ratio is increased from 0.1 to 0.4, there is a remarkable increase (approximately 110%) in Nu_{avg} for a constant Hartmann number such as Ha = 300.
- Snapshots of isotherms for the different Hartmann numbers and blockage ratios confirm that increasing of blockage ratio and reducing the Hartmann number improves the cold and hot fluids mixing and subsequently further enhances heat transfer from the heated wall of the channel.

Nomenclature

a – channel height, [m]
B – magnetic field, [T]
C_D – drag coefficient
d – obstacle chord length, [m]
f – vortex shedding frequency, [Hz]
h – channel height, [m]
Ha – Hartmann number
J – Joule heating parameter
k – thermal conductivity, [$Wm^{-1}k^{-1}$]
L_b – re-circulation length
N – Stuart number
Nu – Nusselt number
Pr – Prandtl number
Re – Reynolds number
Re_c – critical Reynolds number
Re_m – magnetic Reynolds number
St – Strouhal number
T_w – temperature at the channel wall, [K]
X_u – dimensionless upstream distance
X_d – dimensionless downstream distance

Greek symbols

β – blockage ratio
γ – aspect ratio (= a/h)
θ – dimensionless temperature
ν – kinematic viscosity, [m^2s^{-1}]
ρ – density, [kgm^{-3}]
σ – electrical conductivity, [Ωm]

Subscript

nd – non-dimensional

References

[1] Sommeria, J., Moreau, R., Why, how, and when, MHD Turbulence Becomes Two-Dimensional, *Journal of Fluid Mechanics*, *118* (1982), May, pp. 507-518
[2] Potherat, A., *et al*., An Effective Two-Dimensional Model for MHD Flows with Transverse Magnetic Field, *Journal of Fluid Mechanics*, *424* (2000), Dec., pp. 75-100
[3] Krasnov, D., *et al*., Numerical Study of Magnetohydrodynamic Duct Flow at High Reynolds and Hartmann Numbers, *Journal of Fluid Mechanics*, *704* (2012), Aug., pp. 421-446
[4] Dousset, V., Potherat, A., Numerical Simulations of a Cylinder Wake under a Strong Axial Magnetic Field, *Physics of Fluids*, *20* (2008), 1, pp. 017104-017116
[5] Hussam, W. K., *et al*., Dynamics and Heat Transfer in a Quasi-Two-Dimensional MHD Flow Past a Circular Cylinder in a Duct at High Hartmann Number, *International Journal of Heat and Mass Transfer*, *54* (2011), 5-6, pp. 1091-1100
[6] Frank, M., *et al*., Visual Analysis of two-Dimensional Magnetohydrodynamics, *Physics of Fluids*, *13* (2001), 8, pp. 2287-2295
[7] Hussam, W. K., *et al*., Optimal Transient Disturbances behind a Circular Cylinder in a Quasi-Two-Dimensional Magnetohydrodynamic Duct Flow, *Physics of Fluids*, *24* (2012), 2, pp. 024105-024116
[8] Vetcha, N., *et al*., Study of Instabilities and Quasi-Two-Dimensional Turbulence in Volumetrically Heated Magnetohydrodynamic Flows in a Vertical Rectangular Duct, *Physics of Fluids*, *25* (2013), 2, pp. 024102-024126
[9] Muck, B., *et al*., Three-Dimensional MHD Flows in Rectangular Ducts with Internal Obstacles, *Journal of Fluid Mechanics*, *418* (2000), 1, pp. 265-295
[10] Kanaris, N., *et al*., Three-Dimensional Numerical Simulations of Magnetohydrodynamic Flow Around a Confined Circular Cylinder under Low, Moderate, and Strong Magnetic Fields, *Physics of Fluids*, *25* (2013), 7, pp. 1-29
[11] Hussam, W. K., Sheard, G. J., Heat Transfer in a High Hartmann Number MHD Duct Flow with a Circular Cylinder Placed Near the Heated Side-Wall, *International Journal of Heat and Mass Transfer 67* (2013), Dec., pp. 944-954
[12] Morley, N. B., *et al*., GaInSn Usage in the Research Laboratory, *Review of Scientific Instruments*, *79* (2008), 5, pp. 1-3
[13] Thompson, J. F., *et al*., Numerical Grid Generation: Foundations and Applications, Elsevier North-Holland, Inc., New York, USA, 1985
[14] Hoffmann, K. A., Computational Fluid Dynamics For Engineers, Engineering Education System, Austin, Tex., USA, 1993

Paper submitted: March 13, 2014
Paper revised: January 27, 2015
Paper accepted: March 29, 2015

© 2017 Society of Thermal Engineers of Serbia
Published by the Vinča Institute of Nuclear Sciences, Belgrade, Serbia.
This is an open access article distributed under the CC BY-NC-ND 4.0 terms and conditions